

This is the accepted manuscript made available via CHORUS. The article has been published as:

Contribution of thermally scattered electrons to atomic resolution elemental maps

B. D. Forbes, A. J. D'Alfonso, R. E. A. Williams, R. Srinivasan, H. L. Fraser, D. W. McComb, B. Freitag, D. O. Klenov, and L. J. Allen

Phys. Rev. B **86**, 024108 — Published 18 July 2012

DOI: [10.1103/PhysRevB.86.024108](https://doi.org/10.1103/PhysRevB.86.024108)

The contribution of thermally scattered electrons to atomic resolution elemental maps

B.D. Forbes,¹ A.J. D'Alfonso,¹ R.E.A. Williams,² R. Srinivasan,²
H.L. Fraser,² D.W. McComb,² B. Freitag,³ D.O. Klenov,³ and L.J. Allen¹

¹*School of Physics, University of Melbourne, Parkville, Victoria 3010, Australia*

²*Department of Materials Science and Engineering, The Ohio State University,*

477 Watts Hall, 2041 College Road, Columbus, OH 43210, USA

³*FEI Company, Building AAE, Achtseweg Noord 5, Eindhoven, The Netherlands*

(Dated: July 2, 2012)

Electron energy-loss spectroscopy (EELS) and energy dispersive x-ray (EDX) analysis in scanning transmission electron microscopy (STEM) have the ability to produce elemental maps of a specimen at atomic resolution. In this paper we present EELS and EDX maps for the oxygen K-shell in $\langle 001 \rangle$ strontium titanate. The results initially seem to be anomalous since substantially more signal is obtained when the STEM probe is above the columns containing both titanium and oxygen than those containing only oxygen. This is at variance with the stoichiometry - the density of oxygen in both types of columns is the same. Using theory, we show that an understanding of the direct contribution to the recorded signal from electrons which have been thermally scattered is the key to understanding these results. We contrast these results to elemental maps of $\langle 110 \rangle$ strontium titanate. Whilst the experimental results are not directly interpretable, they are in concert with simulations from first-principles such as those presented in this paper.

PACS numbers: 61.05.jd

I. INTRODUCTION

Elemental mapping in two dimensions at atomic resolution using core-loss electron energy-loss spectroscopy (EELS) has been under development since 2007¹⁻⁴ and is now at the point where it can be used to solve problems of technological interest⁵. As an alternative to EELS one can use energy-dispersive x-ray (EDX) analysis, detecting the x-rays which are emitted subsequent to ionization. EDX elemental mapping is an incoherent mode of imaging, as is the widely used technique of Z-contrast imaging, but with the advantage that elemental information is directly available for a range of different elements and x-ray peaks. An advantage of EDX mapping relative to EELS is the accessibility of higher energy-loss peaks and their associated increased localization. The first two-dimensional atomic resolution elemental maps based on EDX were published as recently as 2010^{6,7} and considerable improvements in the quality of such data has followed⁸.

Atomic resolution maps obtained in EELS are based on detecting electrons that have lost energy on transiting through the specimen due to inelastic scattering and which are scattered into a range of angles in the forward direction, defined by the collection aperture of the spectrometer. We then consider the integrated signal from a subset of those electrons falling into a suitable energy-loss window above the threshold energy for a particular core-loss edge. When detecting x-rays associated with a particular edge in the EDX imaging mode, all possible kinematics of the inelastically scattered fast electron are effectively sampled since there is no restriction to scattering in the forward direction imposed by the EELS spectrometer. In addition, the energy window effectively extends over all possible energies above the threshold.

So we expect that EELS with a large detector aperture and a large energy window, starting at threshold, would have similar underlying physics to EDX-based elemental mapping.

The similarity in the underlying physics for EDX and EELS mapping is borne out by the results we will discuss shortly in Sec. II. Apparently anomalous behaviour is seen in both EELS and EDX elemental maps for the oxygen K-shell signal in $\langle 001 \rangle$ strontium titanate: substantially more signal is obtained when the STEM probe is above columns containing both titanium and oxygen when compared with those containing only oxygen, despite the density of oxygen in both types of columns being the same (one atom per 3.905 Å). Precisely this effect has also been noted in previous work by Dudeck and coworkers⁹.

II. EXPERIMENTAL DATA

The EELS data were obtained at Ohio State University. Figure 1 shows a line scan taken across successive Ti/O and O columns which shows the substantially enhanced signal on the Ti/O columns compared with that on the O columns. The data were collected at an accelerating voltage of 300 kV on an aberration corrected FEI Titan with a probe-forming convergence semi-angle of approximately 17 mrad and a collection semi-angle at the detector of 35 mrad. An energy window of 40 eV above the edge onset was used. The thickness of the specimen was estimated to be 200 Å.

Elemental mapping using EDX was also performed on $\langle 001 \rangle$ strontium titanate at FEI Company in Eindhoven. An aberration corrected Titan G2 microscope equipped with a Super-X detector⁸ was used. The accelerating

voltage was 200 kV and the probe-forming convergence semi-angle was approximately 23 mrad. The specimen thickness in this case was somewhat greater, approximately 700 Å. The same apparently anomalous behaviour seen in EELS was noted when detecting x-rays associated with the K-shell edge. A map for a single two-dimensional scan based on the oxygen K edge (raw data) is shown in Fig. 2(a) whereas a filtered average using a 5×5 pixel moving-average square window is shown in Fig. 2(b). A substantial enhancement of the signal on the Ti/O columns relative to the pure O columns is once again evident.

Considering thermal diffuse scattering, which is expected to redistribute the electron flux away from the column, one might initially argue that, for both the EELS and EDX cases, a lower signal should be obtained when the probe is on the Ti/O columns than when it is on the O columns. This view seems reasonable on the basis of previously reported EELS elemental maps, where it was seen that thermal diffuse scattering can reduce the signal from a column relative to off-column probe positions, explained by the depletion of the elastically scattered probe on the column by thermal scattering^{1,10}. However the data in Figs. 1 and 2 clearly show that, in this case, the opposite is true. This is consistent with the results of a coeval study by Dudeck et al.⁹, who observed that EELS maps of oxygen in strontium titanate did not appear to reflect the stoichiometry but offered no explanation for the observation.

We will show that the contribution to the signal from thermally scattered electrons (those which have already excited a phonon, perhaps multiple times) is key to understanding the enhancement of the signal seen in the experimental data when the probe is on the column containing the heavier Ti atoms. This is due to ionization by the thermally scattered electrons of oxygen atoms surrounding the column (and quite far from it in some cases). This insight is made possible by using the recently introduced model for thermal scattering which employed a Born-Oppenheimer (BO) approximation to solve the quantum mechanical many body problem¹¹. This model allows one to track the contribution to the measured signal from both elastically and thermally scattered electrons separately, unlike the widely used frozen phonon model for thermal scattering^{12,13}. It is precisely the ability to consider each of these contributions that throws light on the crucial role of the thermally scattered electrons.

III. THEORY

In the Born-Oppenheimer approximation model¹¹ the cross section for ionization as a function of probe position is obtained by a suitably weighted averaging of contributions from the many possible configurations of the crystal seen by a *single* incident electron. The fraction of the incident electrons which undergo inelastic scattering due to

ionization can be expressed in the form^{11,14–16}

$$I(\mathbf{R}, t) = \frac{1}{A^2} \sum_{j=1}^J \int_0^t \int_A \int_A \phi_j^*(\mathbf{R}, \mathbf{r}_\perp, z) \times W(\mathbf{r}_\perp, \mathbf{r}'_\perp) \phi_j(\mathbf{R}, \mathbf{r}'_\perp, z) d\mathbf{r}_\perp d\mathbf{r}'_\perp dz. \quad (1)$$

The position of the STEM probe is denoted by \mathbf{R} , t is the thickness of the specimen (along z), A is the area of the unit cell, j labels a particular configuration of the atoms in the crystal and J denotes the number of different configurations used. The probe function associated with the configuration j at a depth z is given by $\phi_j(\mathbf{R}, \mathbf{r}_\perp, z)$, where the co-ordinate \mathbf{r}_\perp is in the plane perpendicular to the z direction. In general the effective potential $W(\mathbf{r}_\perp, \mathbf{r}'_\perp)$ for inelastic scattering, in this case due to ionization, is nonlocal since it depends on the two co-ordinates \mathbf{r}_\perp and \mathbf{r}'_\perp . The signal also depends on the probe function at both \mathbf{r}_\perp and \mathbf{r}'_\perp . This means that the relative phase of the probe function at points \mathbf{r}_\perp and \mathbf{r}'_\perp is relevant.

The projected nonlocal potential $W(\mathbf{r}_\perp, \mathbf{r}'_\perp)$ has the form

$$W(\mathbf{r}_\perp, \mathbf{r}'_\perp) = \frac{2\pi m}{h^2 t} \sum_{\alpha} \sum_{n \neq 0} k_n H_{\alpha, n0}^*(\mathbf{r}_\perp) H_{\alpha, n0}(\mathbf{r}'_\perp) \times \int e^{2\pi i \mathbf{K}'_\perp \cdot (\mathbf{r}_\perp - \mathbf{r}'_\perp)} \delta(k_n - K') d\Omega_{K'} dK', \quad (2)$$

where m is the relativistically corrected electron mass. We have defined the projected transition potential matrix element as

$$H_{\alpha, n0}(\mathbf{r}_\perp) \equiv \int_0^t H_{\alpha, n0}(\mathbf{r}) e^{2\pi i (K - K') z} dz. \quad (3)$$

The modulus squared of the transition potential, $|H_{\alpha, n0}|^2$, gives the probability for inelastic scattering from atom α where ionization occurs from an initial state 0 via the interaction Hamiltonian to a final state n (with wave number k_n for the inelastically scattered electron). The wave number of the incident electron is K (corrected for refraction). The integration over $d\Omega_{K'}$ effectively integrates over all scattered electrons with wave vector $\mathbf{K}' = (\mathbf{K}'_\perp, K'_z)$ that are pertinent to the experiment subject to the requirement that the magnitude of \mathbf{K}' is constrained by conservation of energy to be on the energy shell defined by $K' = k_n$. In Eq. (3) it has been assumed that $K'_z \approx K'$ (a good approximation for scattering which is predominantly in the forward direction). The range of integration over $d\Omega_{K'}$ is determined by the acceptance angle of the detector in EELS and is the whole solid angle for an EDX experiment. For a detector with a large acceptance angle (and therefore always in the EDX case) the effective potential for inelastic scattering becomes local and Eq. (1) reduces to

$$I(\mathbf{R}, t) = \frac{1}{A^2} \sum_{j=1}^J \int_0^t \int_A |\phi_j(\mathbf{R}, \mathbf{r}_\perp, z)|^2 V(\mathbf{r}_\perp) d\mathbf{r}_\perp dz, \quad (4)$$

where $V(\mathbf{r}_\perp)$ is now a local ionization potential which can be explicitly written as

$$V(\mathbf{r}_\perp) = \frac{\pi m}{h^2 t} \sum_{n \neq 0} \frac{1}{k_n} \sum_{\alpha} |H_{\alpha, n0}(\mathbf{r}_\perp)|^2. \quad (5)$$

The propagation of the probe function along z can be calculated using the multislice formulation¹⁴. We emphasize again that Eq. (4) is the total fraction of the incident electrons that undergo inelastic scattering due to ionization, *including* electrons that have already been thermally scattered.

To separate out the contribution to the signal from electrons which have only been elastically scattered prior to ionization, it is important to realize that the wave function $\psi_0(\mathbf{R}, \mathbf{r}_\perp, z)$ for the *elastic* scattering of the probe at depth z can be obtained by a coherent summation of the auxiliary functions $\phi_j(\mathbf{R}, \mathbf{r}_\perp, z)$ ¹¹. We note that it has been shown¹¹ that essentially the same result for $\psi_0(\mathbf{R}, \mathbf{r}_\perp, z)$ can be rapidly obtained using the absorptive model of Hall and Hirsch¹⁷. Consequently the distribution of elastically and thermally scattered electrons can be visualized. Then for the local potential case (a similar approach applies to the more general nonlocal case), the contribution to the total signal from electrons which have been elastically scattered prior to ionization is

$$I_0(\mathbf{R}, t) = \frac{1}{A^2} \int_0^t \int_A |\psi_0(\mathbf{R}, \mathbf{r}_\perp, z)|^2 V(\mathbf{r}_\perp) d\mathbf{r}_\perp dz, \quad (6)$$

Consequently, we are also able to calculate the contribution to the total EELS or EDX signal from electrons which have previously been thermally scattered.

As discussed in the introduction, in the first instance an EDX signal is assumed to be proportional to an EELS signal where the detector is effectively the full solid angle and the energy window encompasses all possible energy losses above the ionization threshold. Fluorescence yields, the absorption of x-rays by the specimen¹⁸ and detector efficiency could also be considered but those refinements will not be taken into account in this paper.

IV. SIMULATIONS AND DISCUSSION

Figure 3 shows simulated EELS and EDX elemental maps of the oxygen K-shell edge in $\langle 001 \rangle$ strontium titanate for the experimental results shown in Figs. 1 and 2, with the simulation parameters in each case being those given in Sec. II. These results are separated into contributions from elastically and thermally scattered electrons, as discussed in Sec. III. At the thicknesses used for these calculations (200 Å for EELS and 700 Å for EDX), the total signal is higher on the titanium-oxygen (Ti/O) columns than on the pure oxygen (O) columns. This is reversed if one only calculates the contribution to the signal from electrons which have only scattered elastically (albeit not by a large amount). It is the contribution

to the signal from electrons which have been thermally scattered prior to ionizing an atom that ensures that the total signal on the Ti/O columns is significantly greater than that on the pure O columns. The fractional intensity for the EDX results in Fig. 3 can be interpreted as an upper bound since, as already pointed out, fluorescence yields and x-ray absorption in the specimen have not been taken into account.

We now investigate how the signal on the Ti/O and the O columns compare as a function of thickness. In Fig. 4 we have plotted the ratio of the total signal when the probe is on the Ti/O columns to that on the pure O columns as a function of thickness. The parameters specified in Sec. II were used to calculate the EELS result in Fig. 4(a) and the EDX result in Fig. 4(b). The ratio is also shown for the contribution from elastically scattered electrons only. It is seen that the ratio of the full contribution is generally not unity, as one would initially anticipate based on stoichiometry. In the EELS case this ratio can be greater than or less than unity depending on the thickness of the specimen. For the EDX case the ratio is always above unity for the range of thicknesses investigated. It is worth noting that changing the probe forming semi-angle to a large value does not bring the ratio closer to unity.

The local approximation for the effective ionization potential is assured for the EDX signal and calculations within that model facilitate discussing the subtleties of what contributes to the signal. So we will continue the discussion with reference to that case. We will now try to understand the results in Fig. 4(b) by considering in detail firstly the contribution to the signal from elastically scattered electrons and then that from electrons which have undergone thermal scattering prior to ionizing an atom.

A. Contribution to the signal from elastically scattered electrons

The separation of the contribution to the EELS or EDX signal from elastically and thermally scattered electrons is possible because the thermally scattered electrons are incoherent with respect to those in the elastic channel. In addition, the contributions to the detected signal from different atoms are mutually incoherent. This means that we can analyze the contribution to the signal when the probe is positioned over a particular column from atoms in that column and atoms in surrounding columns. We will refer to these as on-column and off-column contributions respectively in what follows. This will provide us with insight into where the signals due to elastically scattered electrons and those electrons which have been thermally scattered before ionization are generated in the specimen. In this subsection we consider the former contribution.

Figures 5(a) and (b) show the probe intensity, defined by the flux in the elastic channel, as a function of depth

in the specimen for the probe situated above the Ti/O and O columns. To obtain a sense of scale, the first “lobe” in the probe profile with the probe atop the Ti/O column in Fig. 5(a) encompasses approximately 12 titanium atoms in the vertical direction. These profiles are calculated by taking a one-Å-long line trace through the probe intensity along the [100] direction. Figures 5(c)-(e) are cumulative plots of the component of the EDX signal due to elastically scattered electrons with (c) showing the on-column contributions (d) showing the off-column contributions and (e) indicating the total contribution from all atoms.

In Fig. 5(a) and 5(b), the *Pendellösung* effect seen when the probe is on the Ti/O column is less pronounced on the pure O column, due to the lower average atomic number of that column. On that column the probe is not strongly attracted to the column and hence is not strongly channelled. The intensity when on the Ti/O column is depleted at larger thicknesses due to thermal scattering by the titanium atoms.

A number of aspects should be noted here. Firstly, for this range of thicknesses, the Ti/O column always has a higher on-column contribution. This is what one might expect based on the probe profiles shown. If one plots the derivatives of the curves shown in Fig. 5(c) (not shown here), then the maxima coincide with the “lobes” in the profiles, indicating that *Pendellösung* plays an important role in the strength of this contribution. Secondly, the off-column contribution is consistently higher on the pure oxygen column than on the Ti/O column. This can again be understood by examining the probe profiles. The probe, when positioned over the pure O column, is able to diffuse away from the column and interact with oxygen atoms in surrounding columns. In contrast, the probe is held more tightly on the Ti/O column and thus the off-column contribution is lower. Thirdly, these two tendencies (larger on-column contributions on Ti/O columns due to stronger binding of the probe and larger off-column contributions on pure oxygen due to diffusion of the probe) are at odds with one another, and it is not obvious which should win out over the other. For lower thicknesses one might expect the binding tendency, and thus the Ti/O signal, to dominate, since the probe intensity is already situated around atoms where the ionization potential is peaked, whereas the diffusion to neighbouring O atoms will not occur immediately. Indeed this is the case. For thicknesses up to 600 Å, the total signal in (e) is higher for the probe positioned over a Ti/O column. However, for thicknesses larger than 600 Å the diffusion tendency wins out, and the total signal is higher for the probe positioned over pure oxygen.

At this point we make some more general statements. It appears that the presence of an element of high nuclear charge acts to increase the on-column contribution for elastically scattered electrons. However, such elements may also cause significant thermal scattering, depleting the signal and causing the on-column contribution to saturate. In simple terms, a column with a low aver-

age atomic number appears to allow the probe to diffuse away, resulting in a lower on-column contribution but increasing the off-column contribution. As a means of testing these statements, we will in a later section perform similar calculations for the [110] direction in strontium titanate. This orientation also has both pure O columns and Sr/O columns with a higher average atomic number than the Ti/O columns.

This section has looked only at the contributions to the signal due to ionization by elastically scattered electrons. As seen in Fig. 3(c) and (f), the thermal contribution is also important, and in fact can cause a change in the total relative peak heights compared with the contribution to the signal from elastically scattered electrons. This contribution will be studied in the following section.

B. Contribution to the signal from thermally scattered electrons

The extent to which thermal scattering might contribute to the spectroscopic signal can initially be gauged by examining the fraction of the probe that has been thermally scattered as a function of thickness for various probe positions. This is illustrated in Fig. 6, calculated for the EDX parameters given in Sec. II (briefly, a 23 mrad convergence semi-angle electron probe at 200 kV). It is clear that there is a greater potential for ionization by thermally scattered electrons when the probe is on a Ti/O column than on a pure O column simply because more thermally scattered electrons are generated. The rapid increase in the fraction of electrons that have been thermally scattered (through large angles) when the probe is on a column of Sr is consistent with the fact that there is a significant contribution to the O K-shell signal, despite the lack of O atoms in the Sr column – as can be seen for either EELS or EDX in Figs. 3(c) and (f).

The thermal contribution to the EDX signal is plotted as a function of thickness alongside the elastic and total contributions in Fig. 7. As seen in Fig. 7(b), the contribution from thermally scattered electrons is much greater when the probe is on a Ti/O column than on a pure O column. This, coupled with the contribution for elastic scattering in Fig. 7(a) (a repeat of Fig. 5(a) for ease of comparison) leads to the total signal being consistently larger when the probe is on Ti/O columns as opposed to pure O columns, as seen in Fig. 7(c).

In the previous section, the elastic contributions were divided into on-column and off-column contributions. For the case when the probe is positioned over the Ti/O column, only 14% of the elastic contributions over the 700 Å thickness were off-column. In contrast, here 77% of the contributions from thermally scattered electrons are off-column. Of the total signal recorded for the Ti/O probe position, 33% is contributed by off-column ionization events. The origin of this effect is the large spatial area covered by the thermally scattered electrons (due to the characteristic high-angle scattering).

Figure 8 shows the depth-integrated *real-space* distribution of thermally scattered electrons, with the probe positioned over the Ti/O column. The specimen structure is overlaid, and a logarithmic transformation $x \rightarrow \log(1 + Cx)$, where x is the pixel value and $C = 10^4$, has been applied to the data to highlight interesting features. Prominent radial lines can be seen, and inspection of the overlaid specimen structure shows that the lines correspond to closely-spaced collinear heavy atoms, i.e. those that cause significant thermal scattering. In loose terms, these can be thought of as a real-space analogy of the Kikuchi lines often seen in diffraction patterns.

These radial lines of thermally scattered intensity extend far from the column lying below the probe. As seen in Eq. (4), wherever the intensity overlaps with the ionization potential there will be a contribution to the signal. This confirms that there will be significant contributions from those oxygen atoms lying along the “thermal rays”. These contributions reduce the extent to which the calculated elemental map represents localized information about the specimen structure. The relative peak height recorded for different probe positions also reflects structure containing information from surrounding columns, especially for larger thicknesses ($\gtrsim 200\text{\AA}$ for the case studied here).

C. Different crystal orientation

Let us now consider $\langle 110 \rangle$ strontium titanate as a contrast to the results discussed in Sec. IV A and IV B. In Fig. 9 we show an EDX elemental map for the oxygen K-edge in $\langle 110 \rangle$ strontium titanate, Fig. 9(a) showing the raw data, and Fig. 9(b) a filtered average using a 9×9 pixel moving-average square window. An intensity profile along the line drawn in Fig. 9(b) is shown in Fig. 9(c), and from this figure, we note that the signal on the pure O columns is greater than that on the Sr/O columns. While it is recognized that this profile is not an absolute measure of intensity (because of the averaging technique), this result is not unexpected since the linear density of oxygen atoms in the pure O columns is twice that in the Sr/O columns. Close inspection of the ratio of signals on the two kinds of oxygen columns shows that the ratio is slightly greater than two, as can be seen in Fig. 9(c). However, this is fortuitous and our simulations in Fig. 10, discussed in the next paragraph, show that this will not be true for all specimen thicknesses.

As we did in Sec. IV (see Fig. 4) let us investigate how the signal on the Sr/O and the pure O columns compare as a function of thickness. In Fig. 10 we have plotted the ratio of the total signal when the probe is on the Sr/O columns to that on the pure O columns as a function of thickness. The ratio is also shown for the contribution from elastically scattered electrons only. It is seen that the ratio generally varies from the value of one half that one might expect in view of the fact that the density of oxygen in the Sr/O columns is half that in the pure O

columns. As before, we will now try to understand this by considering in detail firstly the contribution to the signal from elastically scattered electrons and that from electrons which have undergone thermal scattering prior to ionizing an atom.

In Fig. 11 we show calculations equivalent to those in Fig. 5 for the $[001]$ orientation. As before, the Sr/O column elicits strong *Pendellösung*, due to the high average atomic number. Furthermore there is strong depletion of the probe on an Sr/O column due to thermal scattering, which is markedly greater in this case than for a Ti/O column previously. When the probe is above a pure oxygen column it is attracted more strongly to the column, with less diffusion away. This difference is quite marked given that the linear oxygen density only increases by a factor of 1.4 in this orientation relative to the $[001]$ case. These differences manifest themselves as qualitative differences between the elastic signal contributions in Fig. 11(c-e) and those for the $[001]$ orientation in Fig. 5(c-e). The on-column contribution from elastically scattered electrons when the probe is above the Sr/O column is now consistently much less than the on-column contribution when the probe is on the pure O column. Even considering the fact that the latter has twice the oxygen density of the former, this is a significant qualitative change. This results from features discussed above: Sr causes more thermal scattering than Ti, leading to a reduced probe flux on the column and hence a reduced on-column contribution. Furthermore, the increased linear density of oxygen in the pure O columns holds the probe to the columns more effectively, leading to an increased on-column contribution. In this case the off-column elastic contributions are negligible, since on both columns the probe does not get a chance to diffuse away from the probe position.

In Fig. 12 we present calculations equivalent to those for the $[001]$ orientation presented in Fig. 7. Figure 12 (a) is a reprise of the total elastic contribution shown in Fig. 11 (e). In Fig. 12 (b) we see that by comparison with Fig. 7(b), the contribution from thermally scattered electrons is reduced, despite the fact that there is more thermal scattering on the Sr/O column than on the Ti/O. This is due to the way in which these thermally scattered electrons interact with the surrounding specimen structure. To be more specific, for a Ti/O column there is a higher linear density of oxygen atoms and nearby oxygen atoms are closer to the column, where the flux of thermally scattered electrons is higher. A representation of this interaction is shown in Fig. 13, which can be compared with Fig. 8. There are two things to note here. Firstly, there is an enhanced contribution from elastic scattering on the pure oxygen columns, due to the tighter binding of the probe to those columns. Secondly, there is a reduced contribution due to elastic scattering on the Sr/O columns, due to the probe being depleted by thermal scattering. Hence, the role played by the thermal contribution in Fig. 12 (b) is different in this case.

V. CONCLUSION

We have presented apparently anomalous results observed in EELS and EDX elemental maps of the oxygen K-shell edge in $\langle 001 \rangle$ strontium titanate. The relative peak heights observed were not consistent with the fact that the density of oxygen in the mixed Ti/O and pure O columns is the same but, perhaps contrary to expectations the larger signal was on the Ti/O columns. Using the recently developed model for the elastic and thermal scattering of fast electrons in a specimen based on a Born-Oppenheimer approximation, we calculated the contribution to the oxygen K-shell signal from elastically scattered electrons and those which had been thermally scattered (possibly multiple times). It was the latter component which was responsible for the larger signal on the Ti/O column. One can additionally analyze from which atomic columns the elastic and thermal contributions arise. In particular this shows that the contribution to the signal from thermally scattered electrons is quite

delocalized in the sense that there is a considerable contribution from oxygen atoms in columns other than that on which the probe is positioned and at a considerable distance away. We compared those results to an analysis of data for $\langle 110 \rangle$ strontium titanate. The results in this paper underline the crucial role that simulations play in the interpretation of atomic resolution elemental mapping. Experiment *in tandem with* the theoretical models described in this paper can provide a plausible interpretation of structure at the atomic level.

Acknowledgments

This research was supported under the Discovery Projects funding scheme of the Australian Research Council (Project DP110102228) and by the Center for Emergent Materials at the Ohio State University, an NSF MRSEC (Award Number DMR-0820414).

-
- ¹ M. Bosman, V. J. Keast, J. L. García-Muñoz, A. J. D'Alfonso, S. D. Findlay, and L. J. Allen, Phys. Rev. Lett. **99**, 086102 (2007).
 - ² K. Kimoto, T. Asaka, T. Nagai, M. Saito, Y. Matsui, and K. Ishizuka, Nature **450**, 702 (2007).
 - ³ D. A. Muller, L. Fitting Kourkoutis, M. Murfitt, J. H. Song, H. Y. Hwang, J. Silcox, N. Dellby, and O. L. Krivanek, Science **319**, 1073 (2008).
 - ⁴ L. J. Allen, Nature Nanotechnology **3**, 255 (2008).
 - ⁵ S. Trasobares, M. López-Haro, M. Kociak, K. March, F. de La Peña, J. A. Perez-Omil, J. J. Calvino, N. R. Lugg, A. J. D'Alfonso, L. J. Allen, et al., Angewandte Chemie International Edition **50**, 868 (2011).
 - ⁶ A. J. D'Alfonso, B. Freitag, D. Klenov, and L. J. Allen, Phys. Rev. B **81**, 100101R (2010).
 - ⁷ M. W. Chu, S. C. Liou, C. P. Chang, F. S. Choa, and C. H. Chen, Phys. Rev. Lett. **104**, 196101 (2010).
 - ⁸ L. J. Allen, A. J. D'Alfonso, B. Freitag, and D. O. Klenov, MRS Bulletin **37**, 47 (2012).
 - ⁹ K. J. Dudeck, M. Couillard, S. Lazar, C. Dwyer, and G. A. Botton, Micron **43**, 57 (2012).
 - ¹⁰ P. Wang, A. J. D'Alfonso, S. D. Findlay, L. J. Allen, and A. L. Bleloch, Phys. Rev. Lett. **101**, 236102 (2008).
 - ¹¹ B. D. Forbes, A. V. Martin, S. D. Findlay, A. J. D'Alfonso, and L. J. Allen, Phys. Rev. B **82**, 104103 (2010).
 - ¹² R. F. Loane, P. Xu, and J. Silcox, Acta Crystallogr. Sect. A **47**, 267 (1991).
 - ¹³ E. J. Kirkland, *Advanced Computing in Electron Microscopy* (Plenum Press, New York, 1998).
 - ¹⁴ L. J. Allen, S. D. Findlay, M. P. Oxley, and C. J. Rossouw, Ultramicroscopy **96**, 47 (2003).
 - ¹⁵ S. D. Findlay, L. J. Allen, M. P. Oxley, and C. J. Rossouw, Ultramicroscopy **96**, 65 (2003).
 - ¹⁶ S. D. Findlay, M. P. Oxley, S. J. Pennycook, and L. J. Allen, Ultramicroscopy **104**, 126 (2005).
 - ¹⁷ C. R. Hall and P. B. Hirsch, Proc. Roy. Soc. London, Sect. A **286**, 158 (1965).
 - ¹⁸ C. J. Rossouw, C. T. Forwood, M. A. Gibson, and P. R. Miller, Micron **28**, 125 (1997).

Figures

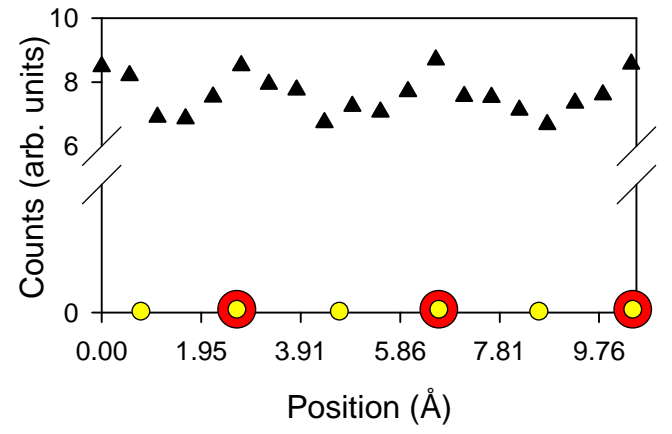


FIG. 1: An EELS line scan from $\langle 001 \rangle$ strontium titanate monitoring the oxygen K-shell signal along successive Ti/O and pure O columns. The experimental conditions are detailed in the text. The density of oxygen in both types of columns is the same in this projection. Nevertheless there is a marked and consistent disparity in the signals. The positions of the Ti/O (red and smaller inset yellow circles) and O columns (small yellow circles) are indicated.

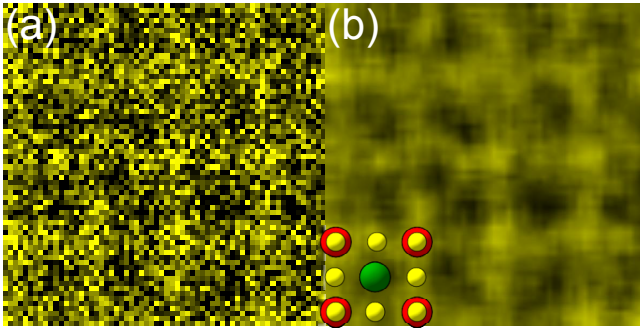


FIG. 2: (a) An EDX elemental map of $\langle 001 \rangle$ strontium titanate monitoring the oxygen K_{α} line for a single scan (raw data). The experimental conditions are given in the text. In (b) the result of applying a 5×5 pixel moving-average square window to the original data is shown. The projected structure is indicated. The positions of Ti/O columns are indicated by the red and smaller inset yellow circles, O columns by small yellow circles and the larger green circle indicates the position of an Sr column.

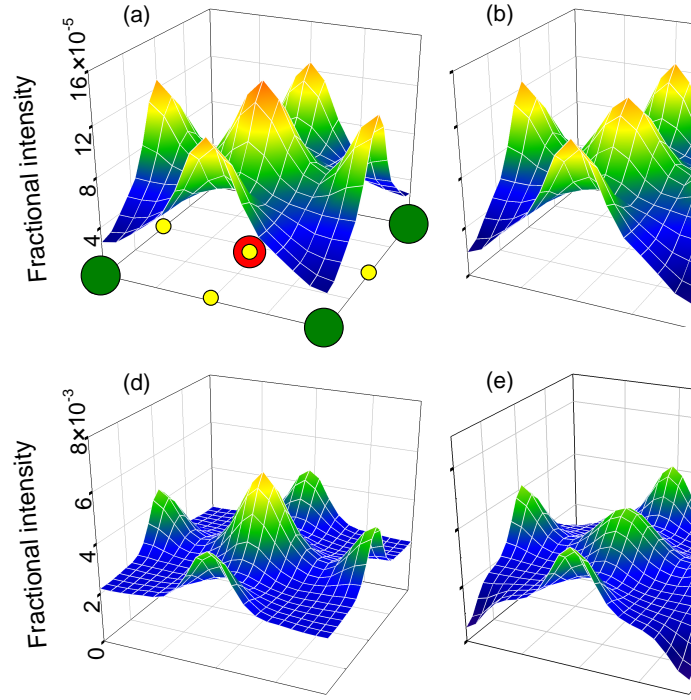


FIG. 3: Simulated elemental maps of the signal in the oxygen K edge in the top row are EELS results for the same imaging conditions pertinent to Fig. 1 (a) shown in (a), the signal for ionization by elastically scattered electrons is shown in (b). The signal for ionization by thermal scattering is in (c). The bottom row shows the calculation chosen, as detailed in Sec. II, to correspond with the experimental data. (d) shows the calculation for ionization by thermal scattering and in (e) that due to ionization by thermal scattering. The positions of the Ti/O column indicated by the red circle in (a) is indicated in (d) with the position of the Ti/O column indicated by the red circle in (e). The O columns by small yellow circles and Sr columns by the large green circle in (d) and (e).

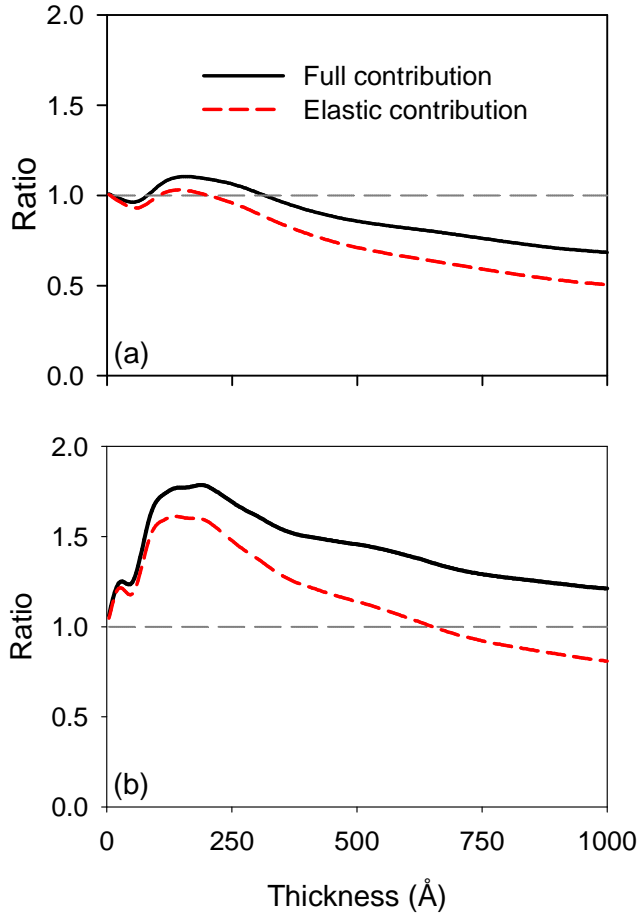


FIG. 4: The ratio of the total oxygen signals on the Ti/O and the O columns as a function of thickness and of the contributions to the signal from elastically scattered electrons only as a function of thickness for (a) the EELS and (b) the EDX case (imaging parameters as specified in Sec. II). Based only on the density of atoms in the Ti/O and O columns one would expect the ratio to be unity in each case.

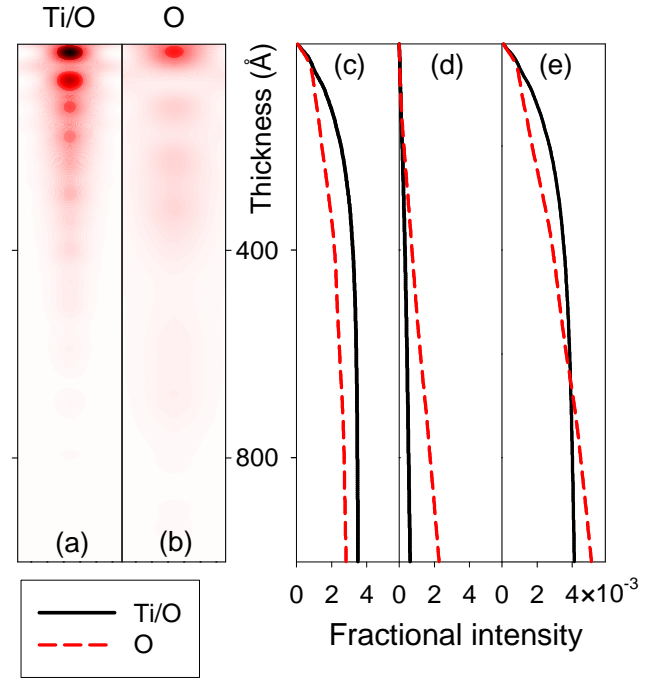


FIG. 5: Calculations of the elastic probe profile in (001) strontium titanate with probe on (a) a Ti/O column and (b) a pure O column. Cumulative plots are shown for the EDX signal for the O K-shell from atoms in the column under the probe (c) and all other columns in (d). The sum of those contributions is plotted in (e). The simulation parameters are as detailed for the EDX experiment in Sec. II.

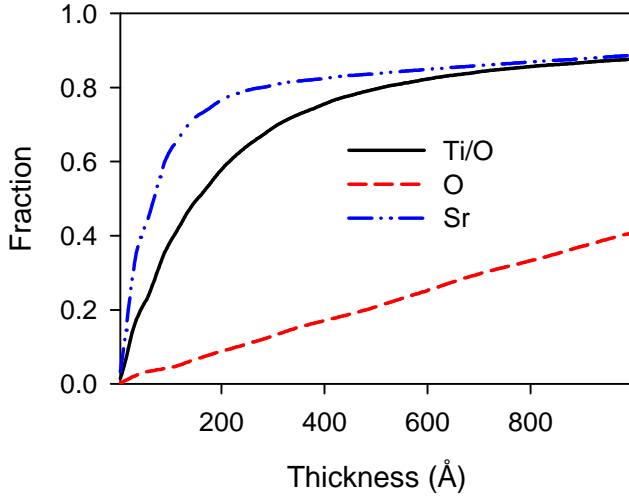


FIG. 6: Fraction of the probe that has been thermally scattered at a given thickness, for probe positions above three different columns of atoms, as indicated, in $\langle 001 \rangle$ strontium titanate. The microscope parameters are those for EDX specified in Sec. II.

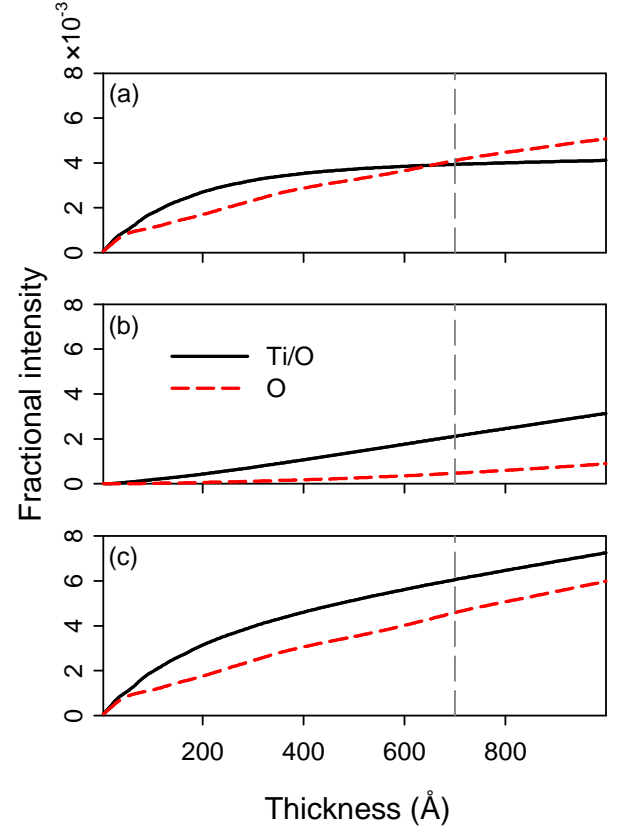


FIG. 7: Contributions to the EDX oxygen K-shell signal in $\langle 001 \rangle$ strontium titanate due to (a) elastically scattered electrons, (b) thermally scattered electrons and (c) all scattered electrons. The calculations were performed for the parameters given in Sec. II. The estimated thickness of the specimen is indicated (700 \AA). Part (a) is the same result as in Fig. 5 (e), repeated here for ease of comparison.

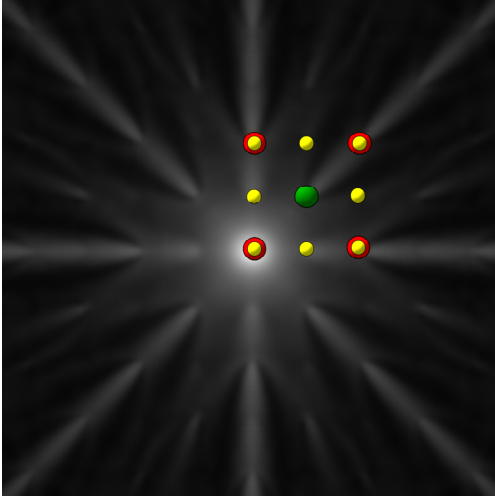


FIG. 8: Depth-integrated *real-space* distribution of thermally scattered electrons for a thickness of 700 Å with the probe positioned over a Ti/O column in (001) strontium titanate. The specimen structure is overlaid. A logarithmic transformation $x \rightarrow \log(1 + Cx)$, where x is the pixel value and $C = 10^4$, has been applied to the calculated results to highlight interesting features.

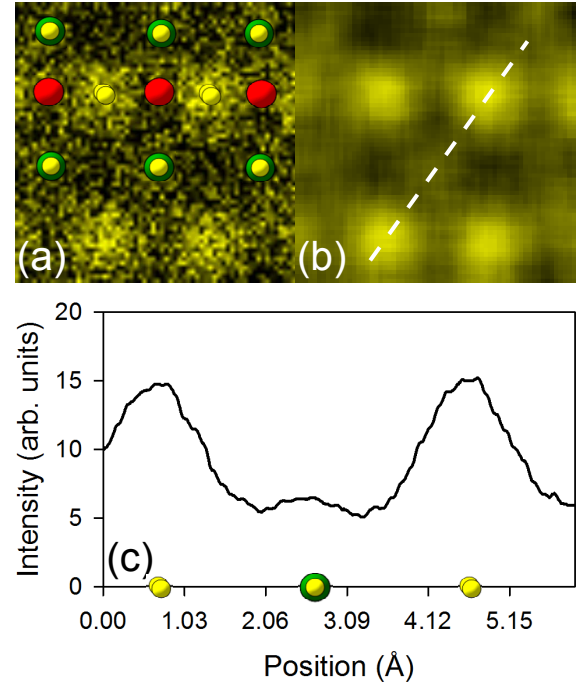


FIG. 9: (a) An EDX elemental map of (110) strontium titanate monitoring the oxygen K-edge for a single scan (raw data). In (b) the result of applying a 9×9 pixel moving-average square window to the original data is shown. In (c) we show a scan across Sr/O and O columns as indicated in (b) (and which had a width of 8 pixels). The projected structure and, in particular, the positions of the Sr/O (green and small inset yellow circles) and O columns (small yellow circles) is indicated. The red circle indicates the position of the Ti column. The experimental parameters are similar to those specified in Sec. II for the data in Fig. 2.

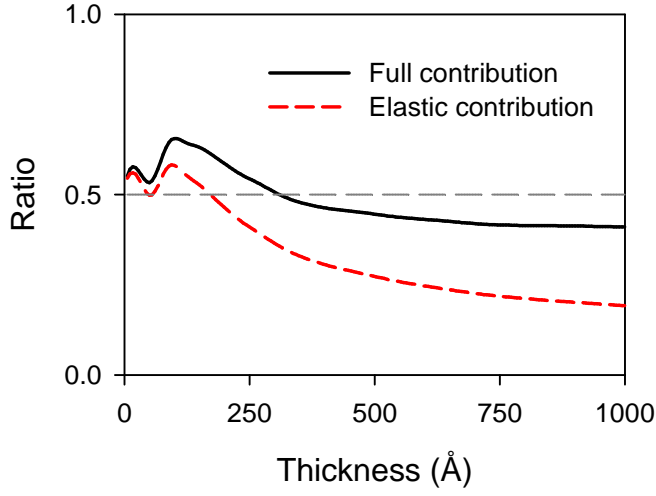


FIG. 10: The ratio of the total oxygen signals on the Sr/O and the O columns as a function of thickness and of the contributions to the signal from elastically scattered electrons only as a function of thickness for the EDX case (imaging parameters as specified in Sec. II). Based only on the density of atoms in the Sr/O and O columns one would naively expect the ratio to be one half.

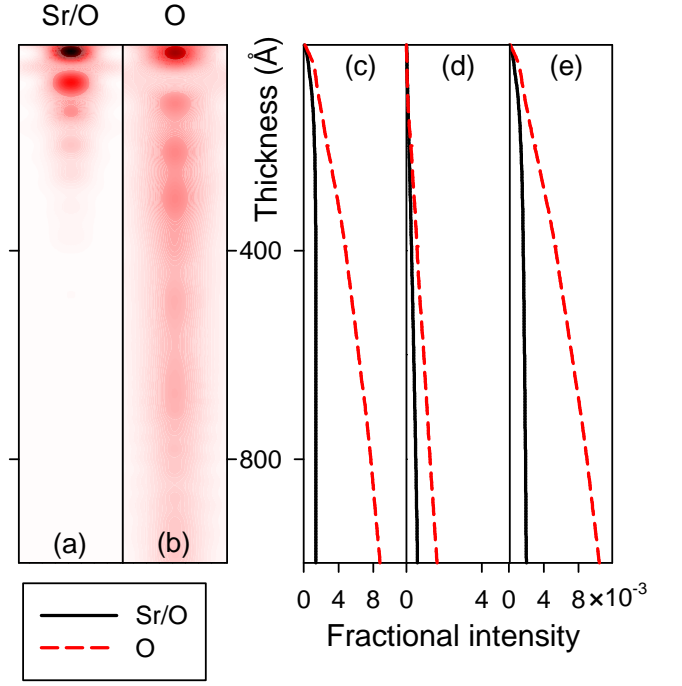


FIG. 11: Calculations of the elastic probe profile in $\langle 110 \rangle$ strontium titanate with probe on (a) a Sr/O column and (b) a pure O column. Cumulative plots are shown for the EDX signal for the O K-shell from atoms in the column under the probe (c) and all other columns in (d). The sum of those contributions is plotted in (e). The simulation parameters are as detailed for the EDX experiment in Sec. II.

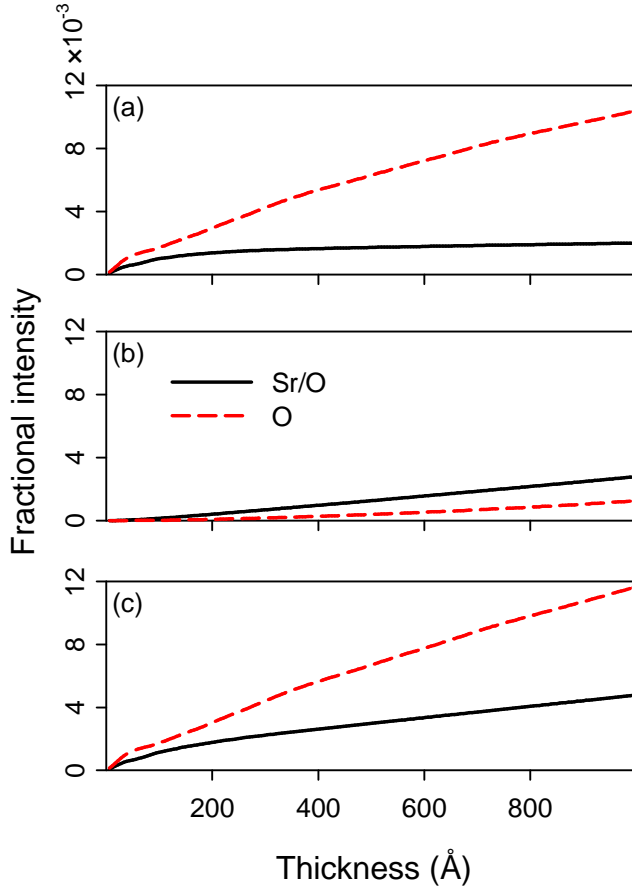


FIG. 12: Contributions to the EDX oxygen K-shell signal in $\langle 110 \rangle$ strontium titanate due to (a) elastically scattered, (b) thermally scattered and (c) all scattered electrons. The calculations were performed for the parameters given in Sec. II. Part (a) is the same result as in Fig. 11 (e), repeated here for ease of comparison.

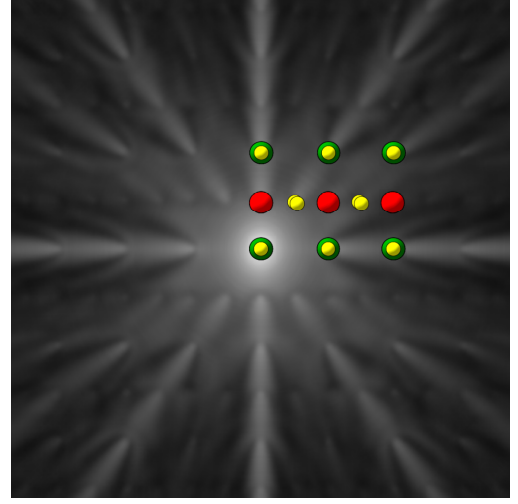


FIG. 13: Depth-integrated *real-space* distribution of thermally scattered electrons for a thickness of 700 Å with the probe positioned over the Sr/O column in $\langle 110 \rangle$ strontium titanate. The specimen structure is overlaid. A logarithmic transformation $x \rightarrow \log(1 + Cx)$, where x is the pixel value and $C = 10^4$, has been applied to the calculated results to highlight interesting features.